International Journal of Nanomedicine

Dovepress
open access to scientific and medical research

Open Access Full Text Article

ORIGINAL RESEARCH

MnO nanoparticles with potential application in magnetic resonance imaging and drug delivery for myocardial infarction

This article was published in the following Dove Press journal:
International Journal of Nanomedicine

Yuanyuan Zheng[1]
Hong Zhang[2]
Yuping Hu[2]
Lu Bai[1]
Jingyi Xue[1]

[1]Department of Pharmacology, School of Basic Medical Sciences, Capital Medical University, Beijing 100069, People's Republic of China; [2]Department of Chemistry and Biology, School of Pharmaceutical Sciences, Capital Medical University, Beijing 100069, People's Republic of China

Background: Myocardial infarction (MI) is a leading cause of death worldwide. Therefore, nanoparticles that applied for specific diagnosis of the infarcted area and/or local myocardial delivery of therapeutic agents, are highly desired.

Materials and methods: Herein, we developed the MnO-based nanoparticles, with magnetic resonance (MR) and near-infrared fluorescence imaging modalities as an MR imaging contrast agent and potential drug vehicle for the detection and treatment of MI. The chemophysical characteristics, targeting ability toward infarcted myocardium, biodistribution, and biocompatibility of the MnO-based nanoparticles were studied.

Results: It was found that the MnO-based dual-modal nanoparticles possess high r_1 relaxivity and induced no notable in vitro or in vivo toxicity. In a rat model of MI, these nanoparticles represent a very promising MR imaging contrast agent for sensitive and specific detection of the infarcted area, more importantly, without cardiotoxicity, the major defect of conventional Mn-based contrasts. Moreover, ex vivo near-infrared fluorescence imaging indicated that the MnO nanoparticles preferentially accumulate in the infarcted myocardium, which makes them an ideal drug vehicle for MI treatment.

Conclusion: In summary, the use of these MnO nanoparticles as a T_1-weighted MR imaging contrast agent and potential drug vehicle to target the infarcted myocardium may provide new opportunities for accurate detection of myocardial infarct and treatment of ischemic heart diseases.

Keywords: Cy5.5 conjugated MnO nanoparticles, Dual-modal nanoprobe, Near-infrared fluorescence imaging, Myocardial ischemia

Introduction

Myocardial infarction (MI) is a major cause of death worldwide. In current clinical practice, the most effective therapy for MI is reperfusion via the occluded coronary artery to control the symptoms, despite its failing to eliminate the disease and inducing additional injuries during ischemia/reperfusion. As a result, many patients eventually develop arrhythmia and/or congestive heart failure.[1] Therefore, it is highly desirable to inhibit myocardial apoptosis and death, and trigger regenerative processes in the infarcted myocardium. Many compounds with good in vitro bioactivity, however, exhibit poor bioavailability, short circulation time, or severe systemic side effects, which strongly limit their applications in the infarct.[2,3] To solve these problems, the most direct approach is the local injection of cardioprotective agents into the infarcted area with or without supportive biomaterial.[4–6] However, direct myocardial injection is extremely invasive and potentially triggers further injury to the weak myocardium.[7] Therefore, emerging noninvasive treatment strategies with intravenous administration of drug delivery systems, or rather, employing nanoparticulate vehicles to encapsulate

Correspondence: Yuanyuan Zheng
Department of Pharmacology, School of Basic Medical Sciences, Capital Medical University, Street of Youanmenwai, #10 Xitoutiao, District of Feng Tai, Beijing 100069, People's Republic of China
Tel +86 10 8391 1836
Fax +86 10 8391 1836
Email zhengyy@ccmu.edu.cn

submit your manuscript | www.dovepress.com
Dovepress
http://dx.doi.org/10.2147/IJN.S176404

therapeutic compounds for local myocardial delivery, to fight against oxidative stress, inflammation, and apoptosis, or to improve angiogenesis represent a promising alternative choice.[8]

On the other hand, for myocardial infarct diagnosis, in addition to the commonly used imaging techniques such as echocardiography, recently magnetic resonance imaging (MRI) is emerging as a favored choice to quantify the amount of necrosis in the myocardium.[9] Currently, Gd-based complexes are dominant contrast agents used in detecting the myocardial infarct.[10] However, Gd-based complexes can easily diffuse not only into necrotic cells through the disrupted plasma membranes, but also into the areas of associated edema; therefore, it causes a potential risk to overestimate the infarct size.[11] Moreover, Gd-based agents are associated with low relaxivity, short half-life, and potential renal risks.[12] Manganese (Mn)-based complexes are alternative MRI contrast agents for infarct imaging not only due to the outstanding paramagnetic property of Mn ions, but also to the capability of entering into cardiomyocytes by L-type voltage-dependant calcium channels and residing in there for hours, which contributes to a selective enhancement of viable cells.[13] However, at present, the use of Mn-based contrast agents is limited by their acute cardiotoxicity due to the free Mn ions released from the agents.[14] Therefore, recently, Mn-based nanoparticles contrasts have been developed to decrease the toxicity and instability and improve biocompatibility.[14,15]

In our previous study, MnO-based nanoparticles with high r_1 relaxivity, long-term colloidal stability, and good performance for the detection of brain gliomas was successfully constructed.[16] However, the ability to diagnose myocardial infarction has not been explored. The conjugation of near-infrared fluorescence (NIRF) to the nanoparticles enables the analysis of biodistribution in the body, particularly in the myocardium at macroscopic level, which makes up for the shortage of MRI. Therefore, in this study, the MR and NIRF dual-modal imaging nanoparticles were employed as an MRI contrast agent and potential drug carrier for estimation of the MI area and targeting the infarcted myocardium for the perspective treatment of myocardial ischemia. Simultaneously, the chemophysical characteristics, biodistribution, and biocompatibility of the MnO nanoparticles were also studied.

Materials and methods

Preparation of MnO-PEG-Cy5.5 nanoparticles

MnO-PEG-Cy5.5 nanoparticles were prepared as previously described.[16] Briefly, the oleic acid-capped MnO (MnO-OA) nanoparticles were first produced by thermal decomposition of manganese oleate at high temperature. Then, by replacing oleic acid with N-(trimethoxysilylpropyl) ethylene diamine triacetic acid, trisodium salt (TETT silane), highly water dispersible MnO-TETT nanoparticles were prepared. Finally, PEG-Cy5.5 was conjugated onto the carboxyl functional groups of TETT silane to accomplish the MnO-PEG-Cy5.5 nanoparticles.

Characterization

A drop of MnO-OA, MnO-TETT, or MnO-PEG-Cy5.5 suspension was placed onto a copper grid to form a thin liquid film. After being dried under vacuum, the size and morphology of the nanoparticles were observed on a transmission electron microscope (JEM-2100F, JEOL, Tokyo, Japan). The X-ray diffraction (XRD) pattern was acquired using an X-ray diffractometer (PANalytical, Almelo, the Netherlands) with Cu target (40 kV, 40 mA). The zeta potential and size distribution (dynamic light scattering, DLS) were determined by a Malvern Nano-ZS90 Zetasizer (Malvern, Worcestershire, UK). The Mn content was measured by an inductively coupled plasma optical emission spectrometer (ICP-OES, Varian 710-ES, Palo Alto, CA, USA). UV–visible spectra were recorded on a UV-2550 spectrophotometer (Shimadzu, Japan). Fluorescence excitation and emission spectra were recorded on an F-2500 fluorescence spectrophotometer (Hitachi, Tokyo, Japan). Fourier transform infrared spectra were also obtained on an IR Prestige-21 spectrophotometer (Shimadzu, Tokyo, Japan).

Relaxivity measurement

The nanoparticles were dispersed in water with Mn concentrations ranging from 0 to 0.5 mM. MRI experiments were performed on a 7.0 T MRI scanner (Bruker Pharmascan, Karlsruhe, Germany). The parameters were as follow: repetition times (TR): 200, 400, 800, 1,500, 3,000, 5,000 ms; echo time (TE) =11.00 ms; slice thickness =1 mm; field of view (FOV) =50×50 mm; matrix =256×256; flip angle (FA) =180.0°.

Cell cultures

Neonatal rat ventricular myocytes (NRVMs) and cardiac fibroblasts (CFs) were isolated from 2-day-old Sprague Dawley rats with 0.1% trypsin and 0.03% collagenase II digestion and cultured, as previously described.[17] H9c2 cells were obtained from the American Type Culture Collection. Cells were cultured at 37°C in DMEM containing 10% fetal

bovine serum and 100 units/mL penicillin/streptomycin in humidified 95% air and 5% CO_2 incubator.

In vitro cytotoxicity

The in vitro cytotoxicity of MnO nanoparticles for NRVMs, CFs, and H9c2 cells was measured by MTT assay. Cells were first cultured in a 96-well plate with DMEM for 24 hours and then starved for 6 hours. Next, cells were treated with different Mn concentrations of nanoparticles (0–100 μM) in the cell medium. After 48 hours of incubation, MTT was added to each well to a final concentration of 0.5 mg/mL and incubated for another 4 hours. The solution was discarded and 150 μL of DMSO was added to each well. Absorbance was measured with a microplate reader (Bio-Rad Model 680, Hercules, CA, USA) at 570 nm.

Ethics statement

All animal care and protocols were approved by the Animal Care Committee of Capital Medical University, Beijing, People's Republic of China (authorization No AEEI-2016–144) and complied with the US Guide for the Care and Use of Laboratory Animals (8th edition, 2011).[18]

Myocardial ischemia surgery

Sprague Dawley rats (males, 200–250 g) were obtained from the experimental animal center of Capital Medical University (Beijing, People's Republic of China). Myocardial ischemia surgery was performed as previously described.[19] Briefly, rats were anesthetized with pentobarbital (intraperitoneal, 40 mg/kg), then intubated, and mechanically ventilated. After the thorax was opened to expose the heart, the left anterior descending coronary artery was permanently ligated. Myocardial ischemia was evaluated by significant elevations of ST segment detected by electrocardiography. Then, the chest was closed and rats were allowed to recover.

In vivo MRI and data analysis

In vivo cardiac MRI scans were performed 1 week after the induction of MI with a 7.0 T MRI scanner. Rats were anesthetized with 2.0% isoflurane and maintained with the mixture of 100% oxygen and isoflurane (1.0%–2.0%). The body temperature was kept at 37°C, and electrocardiogram (ECG) and respiration were continuously recorded by a physiological monitoring system (Small Animal Instruments Inc., Stony Brook, NY, USA). With ECG-triggering and respiratory-gating, short-axis T_1-weighted FLASH sequence (TE =1.8 milliseconds; TR =63 milliseconds; FOV =60×60 mm^2; matrix =256×256; FA =60°; slice thickness =1.5 mm) was performed. Images were obtained at baseline and at 15, 30, 60, and 90 minutes after the injection of MnO nanoparticles at a dosage of 5.0 mg Mn/kg in the tail vein. Regions of interest were targeted on the infarcted area, the remote area, and the background of each image. The contrast-to-noise ratio (CNR) was calculated as $(\mu_r-\mu_i)/\sigma_{noise}$, where μ_r is the mean signal intensity of remote area, μ_i the mean signal intensity of infarcted area, and σ_{noise} the SD of the noise.

Biodistribution

Normal C57BL/6J mice were sacrificed at 4 or 24 hours post intravenous injection of MnO nanoparticles at a dosage of 7.0 mg Mn/kg in the tail vein (n=4 at each time point). The biodistribution of NIR fluorescence in the major organs (heart, liver, spleen, lung, kidney, and brain) was monitored using an Imaging System FX Pro (Kodak, Rochester, NY, USA). The major organs were weighted, dissolved in a mixture of hydrogen peroxide (30%) and nitric acid, and digested by a microwave digest system (CEM, Mars 5, Scotia, NY, USA). Next, the Mn content was determined by ICP-OES (Varian 710-ES, Palo Alto, CA, USA) for each organ.

Confocal imaging of myocardium slices

The hearts of rats were carefully excised, fixed in 4% paraformaldehyde for 24 hours, dehydrated with 30% sucrose, and embedded in OCT (Sakura Finetek, Inc., Torrance, CA, USA). Short axis-oriented cryosections of 5-μm thick were cut for immunofluorescence staining. Slides were blocked with normal goat serum for 1 hour, followed by incubation with primary antibodies overnight. Anti-rat CD18 antibody (Abcam, Cambridge, UK) was used for detection of leukocytes, anti-rat CD68 antibody (Abcam) for macrophages, anti-rat CD31 antibody (Abcam) for blood vessels, and anti-rat laminin antibody (Abcam) for basal membranes. Goat-anti-rabbit Alexa Fluor® 488 (Abcam) or goat-anti-mouse Alexa Fluor® 488 (Abcam) was used as the second antibody. Fluorescently labeled antibodies and Cy5.5 were tracked by a laser scanning confocal microscope (TCS SP5, Leica, Wetzlar, Germany).

In vivo toxicity

C57BL/6J mice were sacrificed 28 days after intravenous injection of MnO nanoparticles at a dosage of 35.0 mg Mn/kg. Mice receiving pure saline were used as the control group (n=6 in each group). The major organs (heart, liver, spleen, lung, kidney, and brain) were collected and immersed with 4% paraformaldehyde for 24 hours, and, after being embedded in paraffin, 5-μm-thick sections of tissues were cut and stained with hematoxylin and eosin.

Results and discussion

Characterization of nanoparticles

First, transmission electron microscopy and DLS were employed to characterize the morphology and size of MnO nanoparticles. It was found that MnO-OA nanoparticles have uniform cubic-like shape with an average DLS size of around 28 nm (Figure 1A), whereas the shape of MnO-TETT and MnO-PEG-Cy5.5 nanoparticles becomes blurred, and the corresponding hydrodynamic diameters increased to around 57 and 60 nm, respectively (Figure 1B and C), indicating the corrosion and aggregation of MnO to some extent due to the modification with TETT. The crystalline structure and phase purity of MnO nanoparticles were next investigated by powder XRD. The featured (111), (200), (220), (311), and (222) peaks in the XRD pattern (Figure 2A) verified the cubic rock salt structure of MnO by referring JCPDS card no 75-0257. Furthermore, Fourier transform infrared spectra of MnO-OA, MnO-TETT, and MnO-PEG-Cy5.5 nanoparticles were acquired to confirm the exchange of OA by TETT and the follow-up conjugation of PEG-Cy5.5. As shown in Figure 2B, all the characteristic bands observed in MnO-OA almost disappeared after TETT modification. In the mean time, new bands at 1,591–1,406 cm^{-1} assigned to COO^-, and 1,328–1,101 cm^{-1} assigned to C–N and Si–C

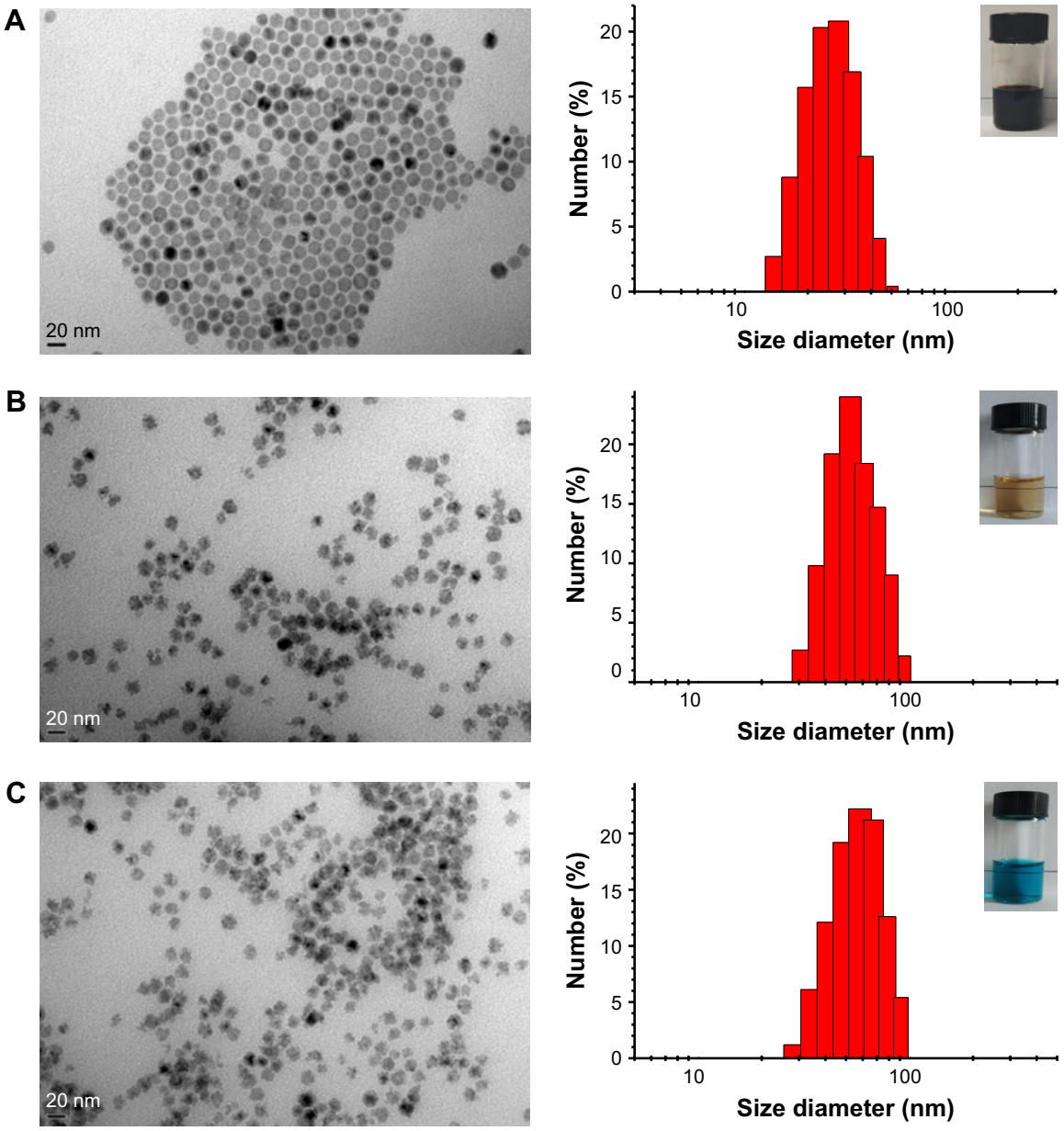

Figure 1 TEM image and size distribution of (**A**) MnO-OA, (**B**) MnO-TETT, and (**C**) MnO-PEG-Cy5.5 nanoparticles.
Notes: Insets showed the pictures of these nanoparticles dispersed in distilled water. Scale bar =20 nm.
Abbreviation: TEM, transmission electron microscopy.

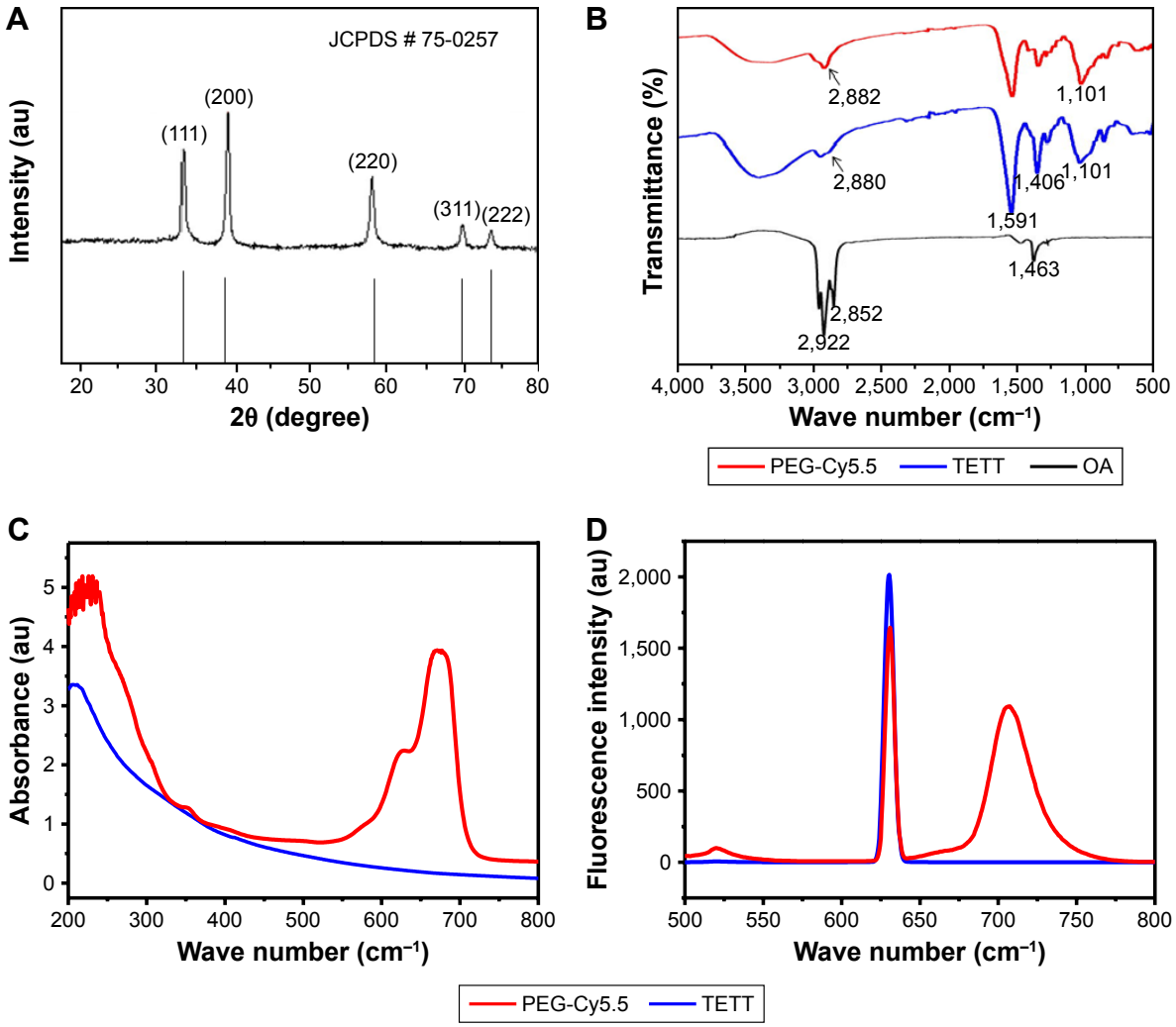

Figure 2 (**A**) XRD pattern of MnO-OA nanoparticles. (**B**) FTIR spectra of MnO-OA, MnO-TETT, and MnO-PEG-Cy5.5 nanoparticles. (**C**) UV-visible absorption spectra and (**D**) Fluorescence emission spectra of MnO-TETT and MnO-PEG-Cy5.5 nanoparticles.
Abbreviations: FTIR, Fourier transform infrared spectra; TETT, N-(Trimethoxysilylpropyl) ethylene diamine triacetic acid; XRD, X-ray diffraction.

stretching vibrations were observed, confirming the exchange of OA by TETT. Comparing to MnO-TETT, the intensity of $-CH_2-$ peak at 2,882 cm^{-1} in MnO-PEG-Cy5.5 became stronger, indicating the conjugation of PEG-Cy5.5. In addition, UV–visible absorption and fluorescence emission spectra of MnO-TETT and MnO-PEG-Cy5.5 nanoparticles were assessed to further verify the conjugation of PEG-Cy5.5 to MnO-TETT. The UV–visible spectra showed MnO-PEG-Cy5.5 nanoparticles displayed strong absorptions at 630 and 675 nm, which were derived from the conjugation of PEG-Cy5.5. As expected, such absorption was not observed for MnO-TETT nanoparticles (Figure 2C). Moreover, the fluorescence emission spectrum of MnO-PEG-Cy5.5 nanoparticles showed an NIR peak at 710 nm upon excitation at 675 nm, whereas MnO-TETT nanoparticles illustrated no peak when excited at the same wavelength (Figure 2D). The conjugated PEG-Cy5.5 onto the MnO nanoparticles was also illustrated by the blue-colored dispersion in water (Figure 1C), which remains stable for weeks. Note that the NIR fluorescence rendered by conjugated PEG-Cy5.5 enables MnO nanoparticles to be visualized in deeper tissues with better signal-to-background ratio. The superimposed excitation and emission spectra for MnO-PEG-Cy5.5 nanoparticles are shown in Figure S1. In addition, the zeta potential of MnO-PEG-Cy5.5 nanoparticles in the medium containing 10% serum (pH 7.4) was measured to be −17.5±1.7 mV.

In vitro and in vivo MRI

To evaluate the effectiveness of MnO nanoparticles as an MRI contrast agent, the relaxivity was measured on a 7.0 T MRI scanner. MnO nanoparticles illustrated a positive T_1 enhancement with a longitudinal relaxivity (r_1) of 4.85 mM^{-1} s^{-1} (Figure 3). The transverse relaxivity (r_2) was 33.58 mM^{-1} s^{-1} (Figure S2), which provides an r_2/r_1 ratio

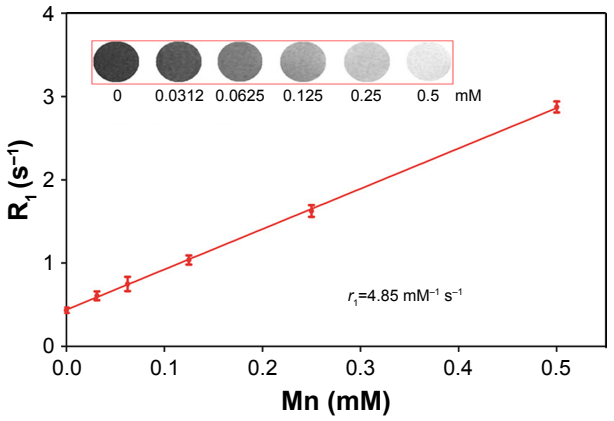

Figure 3 T_1-weighted images and r_1 relaxivity of MnO-PEG-Cy5.5 nanoparticles.
Note: Data are expressed as mean ± SD.

of 6.9. Theoretically, the r_2/r_1 ratio close to unit is desirable for a T_1 contrast agent; nevertheless, this ratio is lower than those previously reported for the Mn-based contrast agents.[20] On the basis of such a high r_1, we evaluated the potential of MnO nanoparticles as an MRI contrast agent for MI imaging in vivo. Representative MR images acquired at basal line and each time point postintravenous injection of the MnO nanoparticles are shown in Figure 4A. Clearly, administration of MnO nanoparticles resulted in hypoenhancement in the infarcted myocardium compared with the viable myocardium at 15–90 minutes postinjection. This result is consistent with the previous studies of Mn-based complexes[21] and could be explained by the following two reasons. First, it is well known that Mn ions are taken up by L-type calcium channels and reside in the viable myocardium for hours, whereas they are quickly washed away from the nonviable myocardium. Second, at the early time points (within 90 minutes postinjection), nanoparticles primarily reside in or around the vascular compartment; however, the infarcted areas are hypoperfused.[22] Corresponding histologic sections stained with Masson displayed the same area of infarct (Figure 4B). The time-curve of CNR in Figure 4C demonstrated significant differences in the cardiac distribution kinetics between viable and infarcted myocardium within the first 90 minutes postinjection. It seems that the remote vs infarcted area generated a slight but not significant increase in CNR (17.7±4.1–22.6±4.1) from 15 to 90 minutes, presumably because more released Mn^{2+} was accumulated in the viable myocardium during this period. These results illustrated that in the rapidly contracting rat heart, Mn distribution in the myocardium could be precisely detected in an MI model using T_1-weighted MRI. In the future, the semiquantitative T_1-weighted MRI might be replaced by quantitative T_1 mapping for a more precise calculation of local Mn concentration,

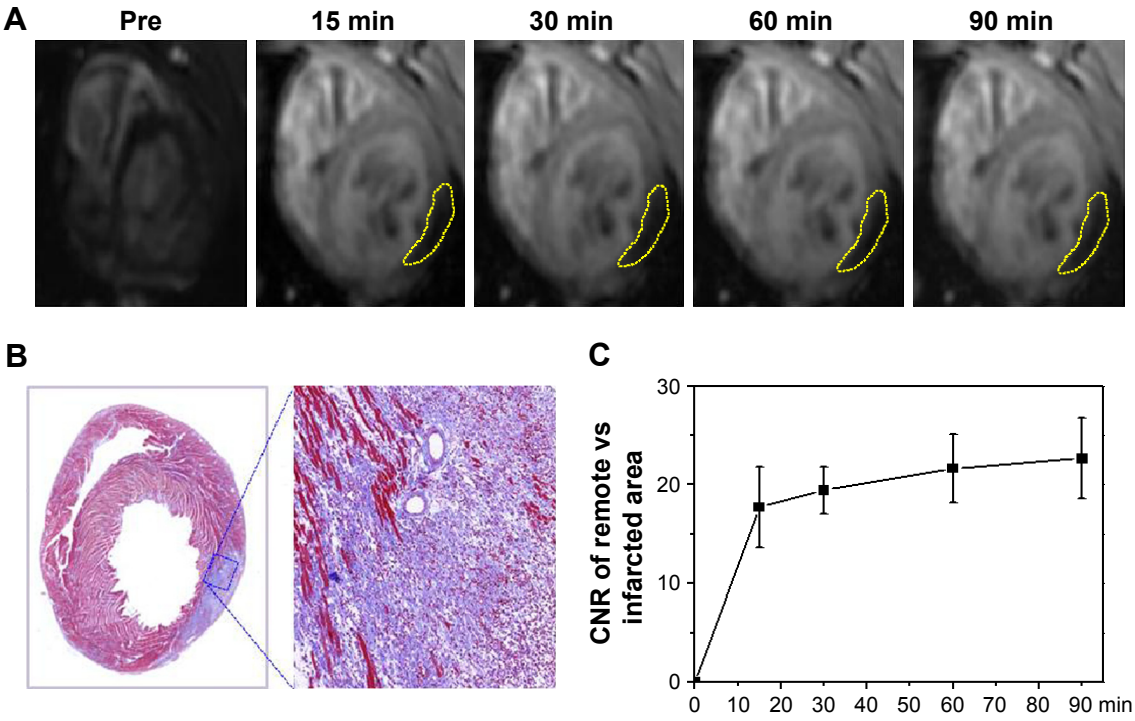

Figure 4 (**A**) Representative in vivo MRI and (**B**) Masson-stained tissue section of the infarcted heart with the administration of MnO-PEG-Cy5.5 nanoparticles by tail vein injection. (**C**) CNR of remote vs. infarcted myocardium of three rats during the first 90 minutes after MnO-PEG-Cy5.5 nanoparticles injection. Data are expressed as means ± SD.
Note: Yellow circles indicate the hypoenhancement of the infarcted myocardium.
Abbreviations: CNR, contrast-to-noise ratio; MI, myocardial infarction; MRI, magnetic resonance imaging.

which could provide us a tool for the more accurate quantification of the infarcted areas.[23]

Confocal imaging of myocardium slices

In addition to serving as a myocardial MRI contrast, the incorporated fluorescent Cy5.5 enables the study of biodistribution and retention of nanoparticles in various organs, especially in the myocardium at a macroscopic level. It is of great interest to develop NIRF-conjugated nanoparticles not only because of their better signal-to-background ratio, but also due to the lower tissue toxicity and autofluorescence compared with other fluorescence probes.[23,24] First, for a more accurate evaluation of the distribution of the MnO nanoparticles in the myocardium, high-resolution confocal laser scanning microscopy was used to monitor the incorporated NIRF on both the infarcted (with ligation surgery) and normal (without ligation surgery) heart. The basal membranes and myofibers (positive staining with laminin), microvasculature (positive staining with CD31), and the inflammatory cells including leukocytes (positive staining with CD18) and macrophages (positive staining with CD68) in the remote regions (viable myocardium) and infarcted regions of the heart were examined in that they are regarded as important indicators for infarct and may also be highly associated with the distribution of nanoparticles in the heart. Data suggested that the density of blood vessels with CD31-positive staining was higher in normal and remote myocardium compared with that in the infarcted area. Macrophages with CD68-positive staining were mostly present in the infarcted areas, whereas leukocytes with CD18-positive staining were comparatively low (Figure 5A).

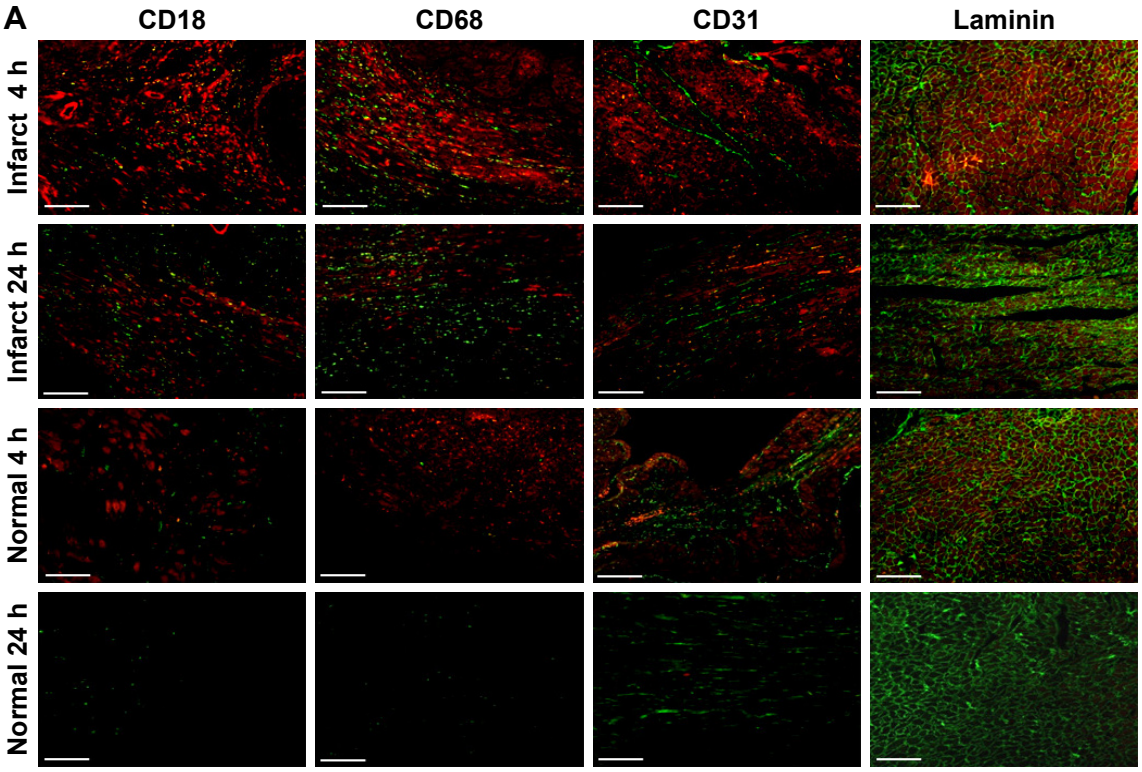

B

	Remote	Infarct	Normal
Nanoparticles (4 h)	+	++	+
Nanoparticles (24 h)	–	+	–
Leukocytes (CD18)	–	+/–	–
Macrophages (CD68)	+/–	++	–
Blood vessels (CD31)	++	+	++

Symbols: – none; +/− low; + moderate; ++ high

Figure 5 (**A**) Ex vivo CLSM images of the infarcted myocardium and normal myocardium at 4 and 24 hours post intravenous injection of MnO-PEG-Cy5.5 nanoparticles. (**B**) Scoring of blood vessels, leukocytes, macrophages and nanoparticles accumulation in the infarcted and remote area of rat MI heart and in the normal myocardium.
Notes: Red: MnO-PEG-Cy5.5 nanoparticles; Green: CD18 (first column), CD68 (second column), CD31 (third column), or laminin (fourth column). Scale bar=100 μm.
Abbreviations: CLSM, confocal laser scanning microscopy; MI, myocardial infarction.

Figure 5B summarizes the quantitative evaluation of NIRF in various areas of the infarcted and normal heart at 4 and 24 hours post nanoparticle injection. Interestingly, nanoparticles showed a notably higher accumulation in the infarcted myocardium compared with that in the remote areas or the normal heart at both 4 and 24 hours postinjection. Costaining with laminin indicated that massive NIRFs were accumulated in the infarcted myocardium, particularly distributed along the necrotic myofibers at 4 hours. More importantly, NIRFs were colocalized with leukocytes and macrophages in the infarcted areas (Figure 5A). This distribution property makes them an ideal delivery vehicle for targeting drugs to the ischemic areas to fight against inflammation, fibrosis, or apoptosis. At 24 hours postinjection, the fluorescence signal in the infarcted area was still detectable, but lower compared with that at 4 hours. In the future, to further improve the recruitment of nanoparticles to the infarct, nanoparticles could be engineered with targets that bind to the infarcted myocardium, such as myosin.[25]

The reasons why MnO nanoparticles in the normal heart showed lower retention compared with the infarcted myocardium at 4 and 24 hours postinjection are probably because of the following two points. First, tissue vasculature becomes increasingly permeable after damage, especially during myocardial ischemia, and such enhanced permeation allows for passive targeting of nanoparticles to the injury.[26,27] Second, the perfusion is partly restored by a quick angiogenic processes after MI, and the newly formed blood vessels are easily permeable to the "nano" characterized drug delivery carriers, which could affect drug biodistribution and retention in various tissues.[28–30] In particular, nanoparticle size partly determines the probability of sequestration by phagocytes and the clearance rate from the circulation system.[4,29] With regard to heart, recent studies suggested a size-dependent effect on nanoparticle retention in the infarcted myocardium and demonstrated that nanoparticles with a diameter within 20–200 nm are optimal for drug delivery on infarcted left ventricle.[6,21] Consistent with the results shown in these studies, the MnO nanoparticles prepared by us with the mean size of 60 nm, which falls in this range, exhibit significant higher retention in the infarcted myocardium compared with the remote area or the normal heart (Figure 5).

Biodistribution

Furthermore, NIRF images of the major organs in healthy mice at 4 and 24 hours post intravenous injection of MnO nanoparticles were also acquired. It was noted that organs harvested at 4 hours postinjection exhibited preferential fluorescence accumulation to kidney, liver, lung, and spleen, and with lower density in heart and brain, whereas the fluorescence could not be detected after 24 hours (Figure 6A). Examination of Mn content by ICP-OES at 4 hours demonstrated a similar biodistribution of MnO nanoparticles in major organs by fluorescence detection. Moreover, ICP-OES exhibited a similar Mn level in the major organs of mice at 24 hours postinjection of MnO nanoparticles or pure saline, indicating that the nanoparticles were almost completely eliminated from the tissues after 24 hours (Figure 6B).

In vitro and in vivo toxicity

The biocompatibility of MnO nanoparticles is also critical for their potential imaging or drug delivery applications. It has been widely reported that Mn-based contrast agents have potential cardiotoxicity resulting from their competitive Ca^{2+} antagonism with effective doses at MR imaging.[31] Although Mn-based nanoparticles have relatively lower toxicity compared with Mn chelates, the small amount of cations released from the nanoparticles may also trigger the toxicity.[32] For example, Chen et al have indicated that their MnO nanoparticles (10 mg Mn/kg) induced notable pathological changes in the lung, liver, and kidney of mice.[33] Singh et al[34] have reported that MnO_2 nanoparticles at a high dose were also able to cause damage in the liver, kidney, and spleen of rats. Herein, considering the myocardial toxicity of Mn^{2+} and the particular target of this drug delivery carrier, cytotoxic effects of the MnO nanoparticles toward cardiomyocytes, including NRVMs and H9c2 cells, and CFs were first evaluated via MTT assay. Figure 7B shows the cell viabilities after 48 hours of incubation with various doses of MnO nanoparticles. Clearly, the viability of each type of cells at all tested concentrations showed no significant difference compared with the control group, indicating that MnO nanoparticles induced no significant cytotoxicity in cardiomyocytes and CFs. Next, we investigated the in vivo toxicity of MnO nanoparticles in healthy mice, which were injected with a single dosage of 35 mg Mn/kg MnO nanoparticles and sacrificed at 28 days after the injection. Histological analysis of the major organs, including heart, liver, spleen, lung, kidney, and brain, was performed with hematoxylin/eosin staining. The results showed that mice receiving a large dose of MnO nanoparticles exhibited no notable inflammation or tissue injury compared to the control group (Figure 7A). Moreover, during the experimental period, animal behaviors, such as neurological status,

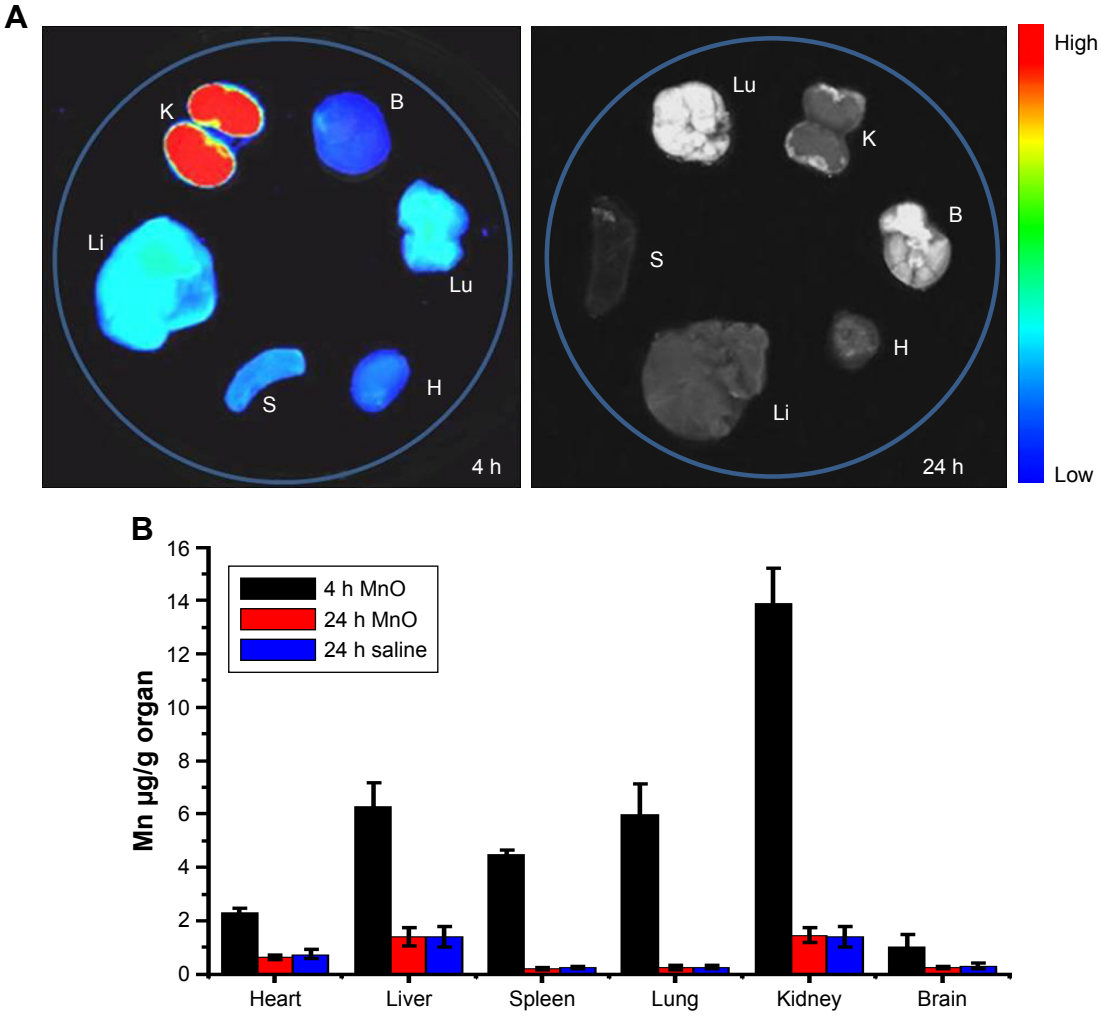

Figure 6 (**A**) NIRF images of major organs from normal mice at 4 and 24 hours post-injection of MnO-PEG-Cy5.5 nanoparticles. (**B**) Mn biodistribution in heart, liver, spleen, lung, kidney and brain of mice at 4 or 24 hours post-injection of MnO-PEG-Cy5.5 nanoparticles or pure saline illustrated by ICP-OES. Data are expressed as means ± SD.
Notes: H, heart; Li, liver; S, spleen; Lu, lung; K, kidney; B, brain.
Abbreviations: ICP-OES, inductively coupled plasma-optical emission spectroscopy; NIRF, near-infrared fluorescence.

exploratory activity, eating, and urination, were observed, and no abnormal animal behavior was found. Together, the in vitro and in vivo data in the current study confirmed the good biocompatibility of our MnO nanoparticles, which thus brings to them a remarkable competitive advantage over the other Mn-based contrast agents. However, more detailed studies are still needed to further evaluate the toxicity of these nanoparticles.

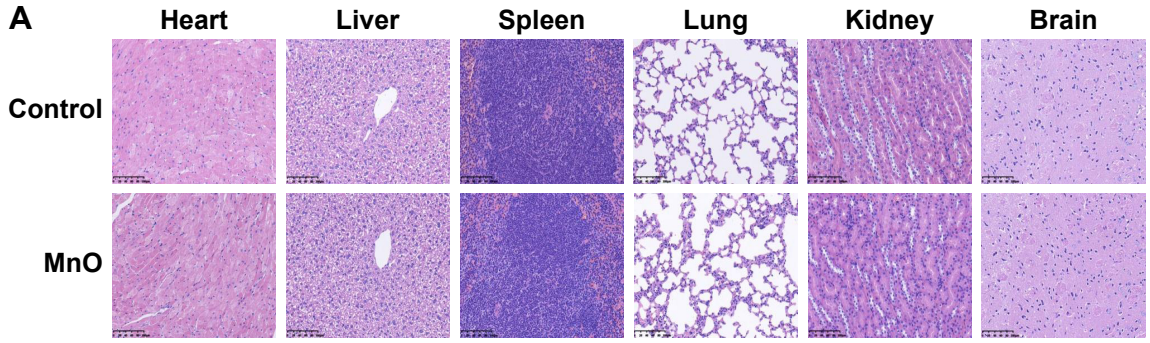

Figure 7 (*Continued*)

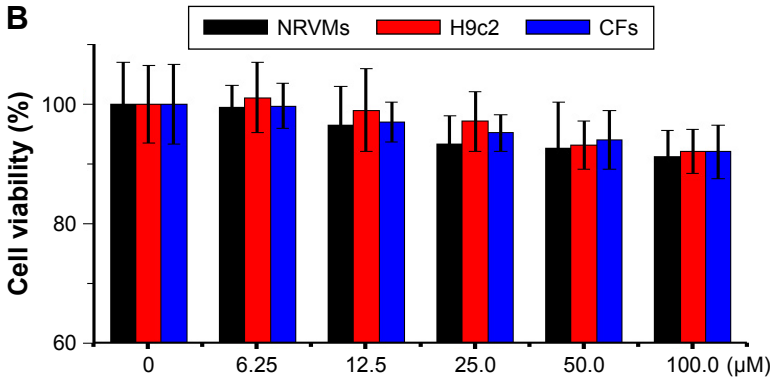

Figure 7 (**A**) HE-stained tissue sections from mice harvested at 28 days after the single injection of pure saline (control) or MnO-PEG-Cy5.5 (35.0 mg Mn/kg), respectively. Tissues were harvested from heart, liver, spleen, lung, kidney and brain. (**B**) Relative viabilities of NRVMs, H9c2, and CFs incubated with various concentrations of MnO-PEG-Cy5.5 nanoparticles (0–100 μM Mn). Data are expressed as means ± SD of four independent experiments.
Note: Scale bar=100 μm.
Abbreviations: CFs, cardiac fibroblasts; HE, hematoxylin-eosin; NRVMs, neonatal rat ventricular myocytes.

Conclusion

In summary, the results indicated that the dual-modality MnO nanoparticles possess high r_1 relaxivity, ideal MR imaging effect for the diagnosis of myocardial infarct, favored infarcted myocardium retention characteristic, and good biocompatibility. The use of these MnO nanoparticles as a T_1-weighted MRI contrast agent or potential drug carrier to target the infarcted myocardium may provide new opportunities for accurate estimation of the infarct size as well as the treatment of ischemic heart diseases. In the future, encapsulation of therapeutic agents in the MnO nanoparticles may improve the accumulation of drugs in the infarcted areas, therefore enhancing the local therapeutic efficacy as well as reducing the harmful systemic side effects.

Acknowledgments

This study was supported by the Beijing Natural Science Foundation (7162027) and Natural Science Foundation of People's Republic of China (81302777).

Author contribution

YZ conceived and designed the research. YZ, HZ, YH, LB and JX performed the experiments. YZ wrote the manuscript. All authors contributed toward data analysis, drafting and critically revising the paper and agree to be accountable for all aspects of the work.

Disclosure

The authors report no conflicts of interest in this work.

References

1. Mersmann J, Latsch K, Habeck K, Zacharowski K. Measure for measure—determination of infarct size in murine models of myocardial ischemia and reperfusion: a systematic review. *Shock*. 2011;35(5):449–455.
2. Scott RC, Rosano JM, Ivanov Z, et al. Targeting VEGF-encapsulated immunoliposomes to MI heart improves vascularity and cardiac function. *FASEB J*. 2009;23(10):3361–3367.
3. Takahama H, Minamino T, Asanuma H, et al. Prolonged targeting of ischemic/reperfused myocardium by liposomal adenosine augments cardioprotection in rats. *J Am Coll Cardiol*. 2009;53(8):709–717.
4. Lundy DJ, Chen KH, Toh EK, Hsieh PC. Distribution of Systemically Administered Nanoparticles Reveals a Size-Dependent Effect Immediately following Cardiac Ischaemia-Reperfusion Injury. *Sci Rep*. 2016;6:25613.
5. Kloner RA. Current state of clinical translation of cardioprotective agents for acute myocardial infarction. *Circ Res*. 2013;113(4):451–463.
6. Chang MY, Yang YJ, Chang CH, et al. Functionalized nanoparticles provide early cardioprotection after acute myocardial infarction. *J Control Rel*. 2013;170(2):287–294.
7. Seif-Naraghi SB, Singelyn JM, Salvatore MA, et al. Safety and efficacy of an injectable extracellular matrix hydrogel for treating myocardial infarction. *Sci Transl Med*. 2013;5(173):ra125.
8. Formiga FR, Pelacho B, Garbayo E, et al. Sustained release of VEGF through PLGA microparticles improves vasculogenesis and tissue remodeling in an acute myocardial ischemia-reperfusion model. *J Control Rel*. 2010;147(1):30–37.
9. Daly C, Kwong RY. Cardiac MRI for myocardial ischemia. *Methodist Debakey Cardiovasc J*. 2013;9(3):123–131.
10. Kim RJ, Albert TS, Wible JH, et al. Performance of delayed-enhancement magnetic resonance imaging with gadoversetamide contrast for the detection and assessment of myocardial infarction: an international, multicenter, double-blinded, randomized trial. *Circulation*. 2008;117(5):629–637.
11. Saeed M, Lund G, Wendland MF, Bremerich J, Weinmann H, Higgins CB. Magnetic resonance characterization of the peri-infarction zone of reperfused myocardial infarction with necrosis-specific and extracellular nonspecific contrast media. *Circulation*. 2001;103(6):871–876.
12. Idée JM, Port M, Dencausse A, Lancelot E, Corot C. Involvement of gadolinium chelates in the mechanism of nephrogenic systemic fibrosis: an update. *Radiol Clin North Am*. 2009;47(5):855–869.
13. Pan D, Caruthers SD, Senpan A, Schmieder AH, Wickline SA, Lanza GM. Revisiting an old friend: manganese-based MRI contrast agents. *Wiley Interdiscip Rev Nanomed Nanobiotechnol*. 2011;3(2):162–173.
14. Wolf GL, Baum L. Cardiovascular toxicity and tissue proton T1 response to manganese injection in the dog and rabbit. *AJR Am J Roentgenol*. 1983;141(1):193–197.
15. Huang H, Yue T, Xu K, Golzarian J, Yu J, Huang J. Fabrication and evaluation of tumor-targeted positive MRI contrast agent based on ultrasmall MnO nanoparticles. *Colloids Surf B Biointerfaces*. 2015;131:148–154.

16. Chen N, Shao C, Li S, et al. Cy5.5 conjugated MnO nanoparticles for magnetic resonance/near-infrared fluorescence dual-modal imaging of brain gliomas. *J Colloid Interface Sci*. 2015;457:27–34.
17. Zheng YY, Zhang HH, Yan XX, et al. Protective effect of low dose gadolinium chloride against isoproterenol-induced myocardial injury in rat. *Apoptosis*. 2015;20(9):1164–1175.
18. National Research Council. *Guide for the Care and Use of Laboratory Animals*. 8th ed. Washington, DC: National Academies Press; 2011.
19. Chen M, Zheng YY, Song YT, et al. Pretreatment with low-dose gadolinium chloride attenuates myocardial ischemia/reperfusion injury in rats. *Acta Pharmacol Sin*. 2016;37(4):453–462.
20. Peng YK, Lai CW, Liu CL, et al. A new and facile method to prepare uniform hollow MnO/functionalized $mSiO_2$ core/shell nanocomposites. *ACS Nano*. 2011;5(5):4177–4187.
21. Toma I, Kim PJ, Dash R, et al. Telmisartan in the diabetic murine model of acute myocardial infarction: dual contrast manganese-enhanced and delayed enhancement MRI evaluation of the peri-infarct region. *Cardiovasc Diabetol*. 2016;15:24.
22. Paulis LE, Geelen T, Kuhlmann MT, et al. Distribution of lipid-based nanoparticles to infarcted myocardium with potential application for MRI-monitored drug delivery. *J Control Rel*. 2012;162(2):276–285.
23. He X, Gao J, Gambhir SS, Cheng Z. Near-infrared fluorescent nanoprobes for cancer molecular imaging: status and challenges. *Trends Mol Med*. 2010;16(12):574–583.
24. Gong H, Kovar JL, Baker B, et al. Near-infrared fluorescence imaging of mammalian cells and xenograft tumors with SNAP-tag. *PLoS ONE*. 2012;7(3):e34003.
25. Khaw BA, Dasilva J, Hartner WC. Cytoskeletal-antigen specific immunoliposome-targeted in vivo preservation of myocardial viability. *J Control Rel*. 2007;120(1–2):35–40.
26. Weis SM. Vascular permeability in cardiovascular disease and cancer. *Curr Opin Hematol*. 2008;15(3):243–249.
27. Goldfarb JW, Arnold S, Han J. Recent myocardial infarction: assessment with unenhanced T1-weighted MR imaging. *Radiology*. 2007;245(1):245–250.
28. He C, Hu Y, Yin L, Tang C, Yin C. Effects of particle size and surface charge on cellular uptake and biodistribution of polymeric nanoparticles. *Biomaterials*. 2010;31(13):3657–3666.
29. Chen KH, Lundy DJ, Toh EK, et al. Nanoparticle distribution during systemic inflammation is size-dependent and organ-specific. *Nanoscale*. 2015;7(38):15863–15872.
30. Dobrovolskaia MA, Aggarwal P, Hall JB, Mcneil SE. Preclinical studies to understand nanoparticle interaction with the immune system and its potential effects on nanoparticle biodistribution. *Mol Pharm*. 2008;5(4):487–495.
31. Bremerich J, Saeed M, Arheden H, Higgins CB, Wendland MF. Normal and infarcted myocardium: differentiation with cellular uptake of manganese at MR imaging in a rat model. *Radiology*. 2000;216(2):524–530.
32. Tian X, Yang F, Yang C, et al. Toxicity evaluation of Gd_2O_3@SiO_2 nanoparticles prepared by laser ablation in liquid as MRI contrast agents in vivo. *Int J Nanomed*. 2014;9(1):4043–4053.
33. Chen R, Ling D, Zhao L, et al. Parallel Comparative Studies on Mouse Toxicity of Oxide Nanoparticle- and Gadolinium-Based T1 MRI Contrast Agents. *ACS Nano*. 2015;9(12):12425–12435.
34. Singh SP, Kumari M, Kumari SI, Rahman MF, Mahboob M, Grover P. Toxicity assessment of manganese oxide micro and nanoparticles in Wistar rats after 28 days of repeated oral exposure. *J Appl Toxicol*. 2013;33(10):1165–1179.

Supplementary materials

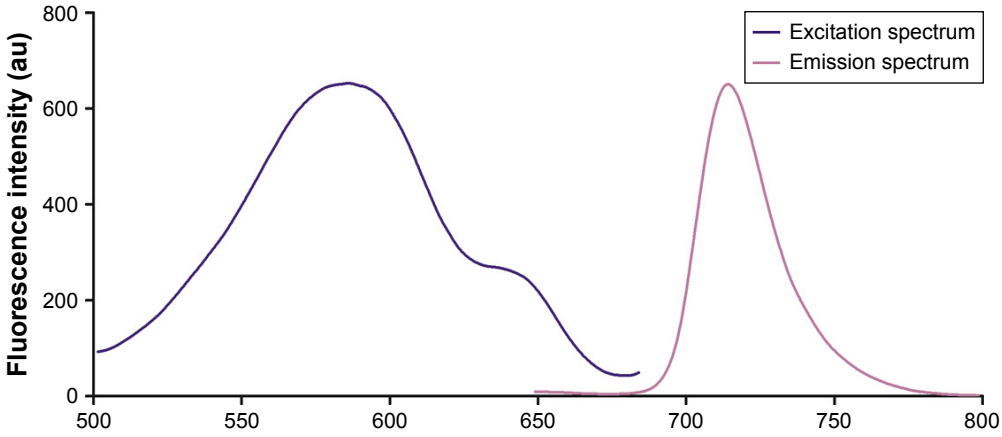

Figure S1 The superimposed excitation and emission spectra for MnO-PEG-Cy5.5 nanoparticles.

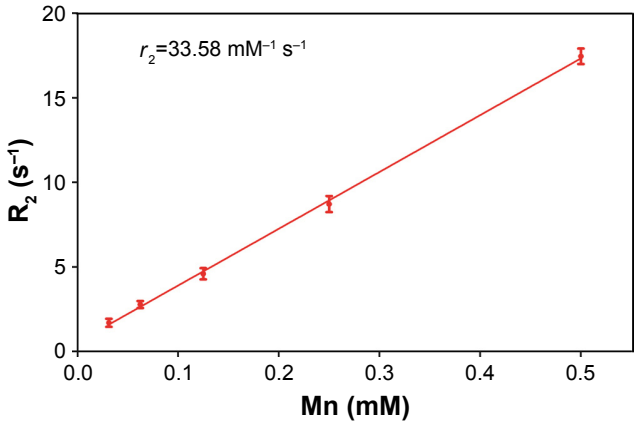

Figure S2 The r_2 relaxivity of MnO-PEG-Cy5.5 nanoparticles.
Note: Data are expressed as mean ± SD.